https://doi.org/10.1007/s11467-023-1371-6

RESEARCH ARTICLE

Efficient conversion of acoustic vortex using extremely anisotropic metasurface

Zhanlei Hao[1,2,*], Haojie Chen[3,*], Yuhang Yin[2,4], Cheng-Wei Qiu[2,†], Shan Zhu[1,‡], Huanyang Chen[1,#]

[1] Institute of Electromagnetics and Acoustics and Department of Physics, College of Physical Science and Technology, Xiamen University, Xiamen 361005, China
[2] Department of Electrical and Computer Engineering, National University of Singapore, 4 Engineering Drive 3, 117583, Singapore
[3] Department of Mechanical and Electrical Engineering, Xiamen University, Xiamen 361005, China
[4] Pen-Tung Sah Institute of Micro-Nano Science and Technology, Xiamen University, Xiamen 361005, China
[*]These authors contributed equally to this work.
Corresponding authors. E-mail: [†]chengwei.qiu@nus.edu.sg, [‡]zhushan@xmu.edu.cn, [#]kenyon@xmu.edu.cn
Received September 3, 2023; accepted November 22, 2023

Supporting information

Section 1: The coupled mode theory for acoustic metasurface (AM)

As is well known, two-dimensional acoustic waves and electromagnetic waves in homogeneous media can be equivalent, and this equivalence also applies to anisotropic media. In two-dimensional coordinate system, for an inviscid fluid with zero shear modulus, the acoustic wave equations are written as follows [1,2]:

$$\rho \frac{\partial \vec{v}}{\partial t} = -\nabla p\,, \tag{S1}$$

$$\frac{\partial p}{\partial t} = -\kappa \nabla \cdot \vec{v}\,, \tag{S2}$$

where p is scalar pressure, $\vec{v}$ is velocity, ρ is mass density, and κ represents bulk modulus. The effective density and bulk modulus of AM satisfy $n(x)=\rho_y=\kappa^{-1}=-(\sqrt{(x-\Delta x)^2+F^2}-F)/L$, $\rho_x\to\infty$. Based on Eqs. S(1) and S(2), we can obtain the acoustic wave form inside AM as follows:

$$p = f(x)e^{ik_0 n(x)y}, v_y = -\frac{k_0}{w} f(x)e^{ik_0 n(x)y}, v_x = 0\,, \tag{S3}$$

where $f(x)$ is the coefficient function with respect to x, $k_0=2\pi/\lambda$ is the wave number in air, and $w=2\pi f$ is the angular frequency.

The proposed AM consists of m=24 unit cells with a width of a. The total length of the acoustic structure is $2p=ma$, the focal distance and the thickness of AM is F and L, respectively. When vortex wave with an OAM of l_{in} is incident on the AM, the entire system is divided into three regions: Region 1, the incident region above the AM; Region 2, the AM region; and Region 3, the transmitted region on below of the AM. Here, we set the coordinate at the center for the upper surface of AM as the origin, and the x-coordinate of each unit cell is given by $x_{\pm j}=\pm(j-1)p/m$. The angle formed between the x-axis and different unit cells corresponds to $\theta_j=\arctan(F/x_j)$, and AM forms an angle α with the transmitted plane wave. The unit cell is filled with the impedance-matched equivalent density material, where the density of the j-th unit cell is given by $n_j=\rho_y=\rho_0 c^2\kappa^{-1}=-(\sqrt{(x-\Delta x)^2+F^2}-F)/L$, $\rho_x\to\infty$, with j ranging from 1 to m.

In the incident region above the AM (Region 1), the incident source is a vortex field with an OAM of l_{in}, given by

$H_{l_{in}}^{(1)}(\bullet)e^{il_{in}\theta}$. Here, $H_{l_{in}}^{(1)}(\bullet)$ represents the l_{in}-th order Hankel function of the first kind, which represents the vortex propagating outward from the center. As a result, the total pressure fields for $y<0$ is the combination of the incident vortex wave and the reflected plane wave as follows:

$$p_1 = [H_{l_{in}}^{(1)}(k_0 r)e^{il_{in}\theta} + r_0 \exp(-ik_y y)]\exp(ik_x x), \quad \text{S(4)}$$

where $ky_j=k_0\sin\theta_j$ and $kx_j=k_0\cos\theta_j$. The complex number r_0 represents the corresponding reflection coefficient. Therefore, the y-components of the velocity fields can be obtained as follows:

$$v_{1y} = \frac{-1}{i\omega\rho_0}[\frac{y+F}{r}H_{l_{in}}^{\prime(1)}(k_0 r)e^{il_{in}\theta} - ik_y r_0 \exp(-ik_y y)]\exp(ik_x x), \quad \text{S(5)}$$

where ρ_0 is air density. In the AM region (Region 2), according to Eq. S(3), the pressure and velocity fields in the j-th medium ($|x-x_j|\le a/2$, $0<y<L$) are written as

$$p_{2,j} = a_j \exp(ik_j y) + b_j \exp(-ik_j(y-L)), (j=1,2\ldots m/2), \quad \text{S(6)}$$

$$v_{2x,j} = \frac{-k_j}{\omega\rho_j}\left[a_j \exp(ik_j y) - b_j \exp(-ik_j(y-L))\right], \left(|x-x_j| \le a/2\right). \quad \text{S(7)}$$

In the above Eqs. S(6) and S(7), the coefficients a_j and b_j are the normalized coefficients representing the amplitude coefficients of plane wave propagating in both the inward and outward directions of the j-th medium. The propagating wave vector in the j-th medium is $k_j=k_0n_j=2\pi n_j/\lambda$.

The pressure and velocity fields for $y>L$ in the transmitted region below the AM (Region 3) can be expressed as

$$p_{3z} = t_0 \exp\left[ik_y'(y-L)\right]\exp(ik_x' x), \quad \text{S(8)}$$

$$v_{3x} = \frac{-k_y'}{\omega\rho_0}t_0 \exp\left[ik_y'(y-L)\right]\exp(ik_x' x), \quad \text{S(9)}$$

where $k_x'=k_0\cos\alpha$ and $k_y'=k_0\sin\alpha$. The function t_0 denotes the corresponding transmission coefficient.

At the boundary $y=0$ between Region 1 and Region 2, with the continuity of the boundary pressure fields, we obtain as follows:

$$(H_{l_{in}}^{(1)}(k_0 r_j)e^{il_{in}\theta} + r_0)\exp(ik_x x) = a_j + b_j u_j, \left(|x-x_j| \le a/2\right), \quad \text{S(10)}$$

where $r_j=\sqrt{x_j^2+F^2}$ and $u_j=\exp(ik_jL)$. Similarly, applying the continuity boundary condition of the velocity field at the boundary $y=0$,

$$\frac{1}{ik_0}[\frac{F}{r_j}H_{l_{in}}^{\prime(1)}(k_0 r_j)e^{il_{in}\theta} - ik_y r_0]\exp(ik_x x) = a_j - b_j u_j, \left(|x-x_j| \le a/2\right). \quad \text{S(11)}$$

At the boundary $y=L$ between the Region 2 and Region 3, we apply the continuity of boundary pressure field, given by

$$t_0 \exp(ik_x' x) = a_j u_j + b_j, \left(|x-x_j| \le a/2\right). \quad \text{S(12)}$$

Likewise, following the continuity boundary condition of the velocity field at the boundary $y=L$, we obtain

$$t_0 \cos\alpha \exp\left(ik_x' x\right) = a_j u_j - b_j, \left(\left|x - x_j\right| \le a/2\right). \quad \text{S(13)}$$

Integrating Eqs. S(10) and S(12) with respect to dx over the region x_j-a/2<x<x_j+a/2, we can obtain

$$(H_{l_{in}}^{(1)}\left(k_0 r_j\right) e^{il_{in}\theta_j} + r_0)\sin c(\frac{k_{xj} w}{2}) \exp\left(ik_{xj} x_j\right) = a_j + b_j u_j, \quad \text{S(14)}$$

$$t_0 \sin c(\frac{k_x' w}{2}) \exp\left(ik_x' x_j\right) = a_j u_j + b_j. \quad \text{S(15)}$$

Furthermore, we can multiply both sides of Eq. S(11) and, as well as Eq. S(13) and, by $e^{-ik_x' x}$, respectively. Integrating both sides with respect to dx over the region 0<x<p, m is as large as possible,

$$\sum_{j=1}^{m} \frac{1}{ik_0} \sin c(\frac{k_{xj} w}{2}) \left(\frac{F}{r_j} H_l'^{(1)}\left(k_0 r_j\right) e^{il\theta_j} - ik_{yj} r_0\right) \exp\left(ik_{xj} x_j\right) = \sum_{j=1}^{m} \left(a_j - b_j u_j\right), \quad \text{S(16)}$$

$$\sum_{j=1}^{m} t_0 \sin c(\frac{k_x' w}{2}) \sin\alpha \exp\left(ik_x' x_j\right) = \sum_{j=1}^{m} \left(a_j u_j - b_j\right). \quad \text{S(17)}$$

It is worth mentioning that a similar derivation process is also applicable to the region -p<x<0. Eventually, we can solve the reflection coefficient r_0 and transmission coefficient t_0. Then, we can calculate the corresponding reflectivity $R=|r_0|^2$ and transmissivity $T=|t_0|^2$.

Section 2: The acoustic experimental design details for vortex converter

To overcome the difficulty of producing vortex wave with larger OAM, the vortex converter using zigzag microstructure is designed to generate vortex waves with different topological charges [3–5]. Specifically, we denote the vortex converters generating vortex sources with OAM of -7 and -14 as CVT-1 and CVT-2 respectively, and the point source with OAM of 0 is formed by arranging 8 loudspeakers in a circular arrangement. The specific working approach is to place the point source at the center of different vortex converters, and they automatically generate vortex wave with different OAM. The different vortex converters are formed by combining the different number of the supercells in a circular arrangement, and a supercell structure shown in Fig. S1(a) is composed of 4 unit cells whose structural parameters are depicted in Fig. S1(c). The transmissivity of each acoustic unit cell is over 97% for generating better the experimental vortex sources, and the phase difference between adjacent unit cells is π/4, as shown in Fig. S1(b). Therefore, we can utilize the designed vortex converter to generate vortex waves with the OAM of -7 and -14 for further acoustic experiment.

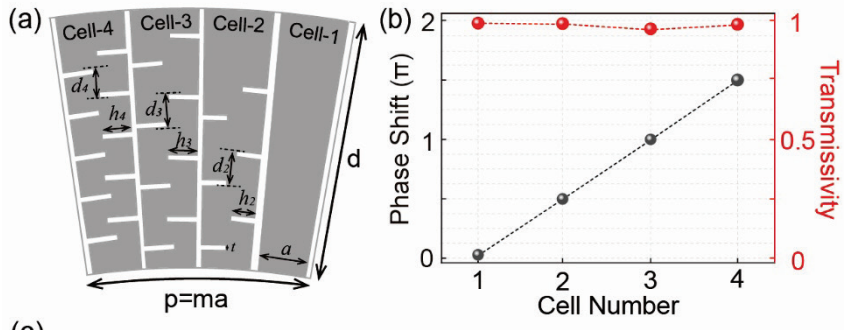

(c)

Number	Distance of Blocks	Height of Blocks	Constants
Cell-1	0	0	t=1.905mm
Cell-2	d_2=5.6t	h_2=0.415(a-t)	a=21.4375mm
Cell-3	d_3=5.3t	h_3=0.505(a-t)	p=72.28mm
Cell-4	d_4=3.6t	h_4=0.520(a-t)	d=85.75mm

Fig. S1 The experimental design detail for a vortex converter supercell. **(a)** Geometric topography of a supercell. **(b)** Phase shift (left) and transmission (right) of the 4 different unit cells. **(c)** Designed parameters for the four different unit cells.

To further validate the working performance of CVT-1 and CVT-2, we conduct the numerical simulations and acoustic experiments to obtain the generated vortex sources with OAM of -7 and -14, as shown in Fig. S2. Specifically, the CVT-1 and CVT-2 are formed by arranging 7 and 14 supercells in a clockwise annular arrangement. By placing the designed point source at the center of vortex converter, they automatically generate vortex wavefronts with OAM of -7 and -14. The simulation results of CVT-1 and CVT-2 generating vortex sources with OAM of -7 and -14 are clearly shown in Figs. S2(a) and (c), and the results of acoustic experiments also produce identical vortex waves patterns, as depicted in Figs. S2(b) and (d). Therefore, both the numerical simulations and acoustic experiments confirm that the plan is feasible to utilize vortex converter to generate vortex sources with different OAM.

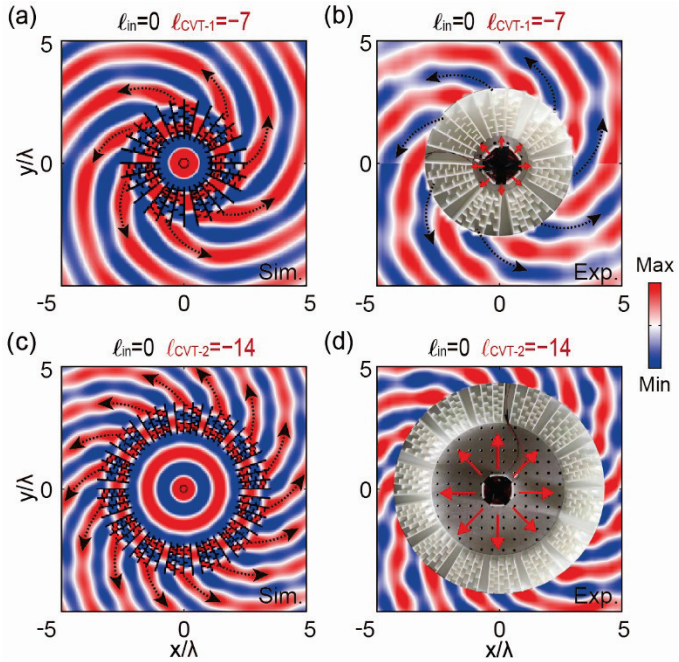

Fig. S2 Numerical and experimental demonstrations of vortex converters. The simulation results: **(a)** $l_{\mathrm{CVT\text{-}1}}$=-7 and **(c)**

l_{CVT-2}=-14. The experimental results: **(b)** l_{CVT-1}=-7 and **(d)** l_{CVT-2}=-14.

Section 3: The acoustic experimental design details for AM sample

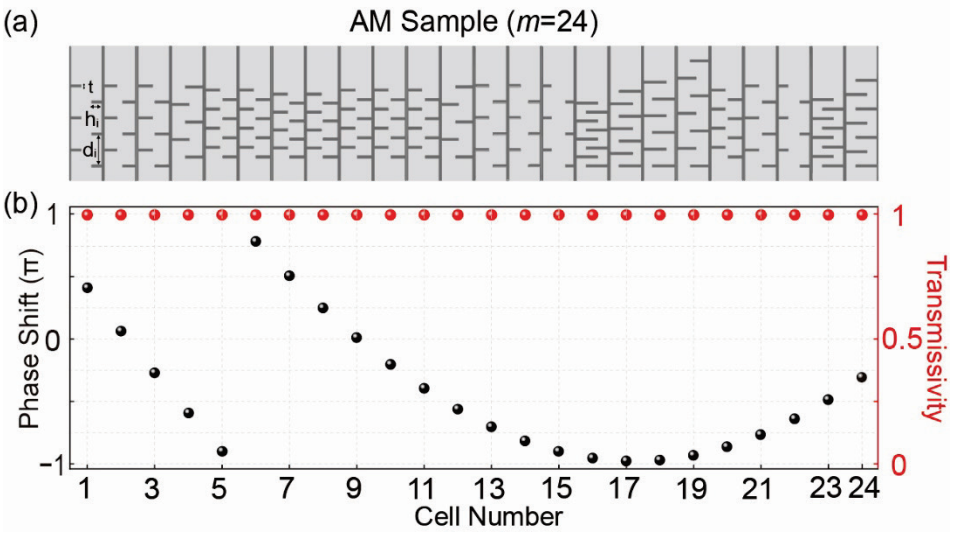

Fig. S3 The experimental design detail for **(a)** AM sample (refer to Table 1 for detailed parameters), and **(b)** the relationship between the phase shift (left) / transmissivity (right) and different unit cells.

As shown in Fig. S3, we design the AM sample using zigzag microstructure [3–5]. The AM sample has a length of $2p=6\lambda$ and a height of $L=\lambda$, which is divided into 24 unit cells, and each with a length of $a=2p/m$. The phase delay and transmissivity of different unit cells are shown in Fig. S3(b), and the transmissivity of each unit cell exceeds 97%. The detailed parameters of each unit cell are listed in Table 1, where the inner wall thickness of the microstructure is t=2mm.

Table 1 Designed parameters for the twenty-four different unit cells.

Number	Distance of blocks	Height of blocks	Number	Distance of blocks	Height of blocks
Cell-1	d1=10.952t	h1=0.334(a-t)	Cell-2	d2=10.952t	h2=0.412(a-t)
Cell-3	d3=10.952t	h3=0.465(a-t)	Cell-4	d4=12.063t	h4=0.566(a-t)
Cell-5	d5=6.147t	h5=0.455(a-t)	Cell-6	d6=6.147t	h6=0.466(a-t)
Cell-7	d7=5.714t	h7=0.474(a-t)	Cell-8	d8=5.714t	h8=0.475(a-t)
Cell-9	d9=6.147t	h9=0.470(a-t)	Cell-10	d10=6.147t	h10=0.461(a-t)
Cell-11	d11=6.147t	h11=0.446(a-t)	Cell-12	d12=12.063t	h12=0.545(a-t)
Cell-13	d13=10.952t	h13=0.440(a-t)	Cell-14	d14=10.952t	h14=0.375(a-t)
Cell-15	d15=10.952t	h18=0.274(a-t)	Cell-16	d16=5.714t	h16=0.069(a-t)
Cell-17	d17=8.278t	h17=0.723(a-t)	Cell-18	d18=11.478t	h18=0.729(a-t)
Cell-19	d19=12.063t	h19=0.596(a-t)	Cell-20	d20=6.147t	h20=0.461(a-t)
Cell-21	d1=10.952t	h21=0.450(a-t)	Cell-22	d22=10.952t	h22=0.314(a-t)
Cell-23	d23=6.081t	h23=0.682(a-t)	Cell-24	d24=9.648t	h24=0.683(a-t)

To verify the manipulation effect of the designed AM sample on vortex waves generated by different vortex converters, we conduct the corresponding experimental simulations on the combination of the AM sample and vortex converters, as shown in Fig. S4. Specifically, the designed point source placed at the center of vortex converters is converted into vortex wave with OAM of -14 after passing through CVT-2, and the AM further convert the vortex wave into a plane wave with deflection angle of -17.35°, as shown in Fig. S4(a). Similarly, the designed AM can also convert the vortex wave with OAM of -7 generated by CVT-1 into vertical plane wave, as depicted in Fig. S4(b). In addition, when only point source is incident, we can observe the plane wave with deflection angle of 16.51° in the transmitted region, as shown in Fig. S4(c). Therefore, from acoustic experimental simulation perspective, we confirm that the designed AM sample can achieve efficient conversion of vortex waves with different OAM to plane waves.

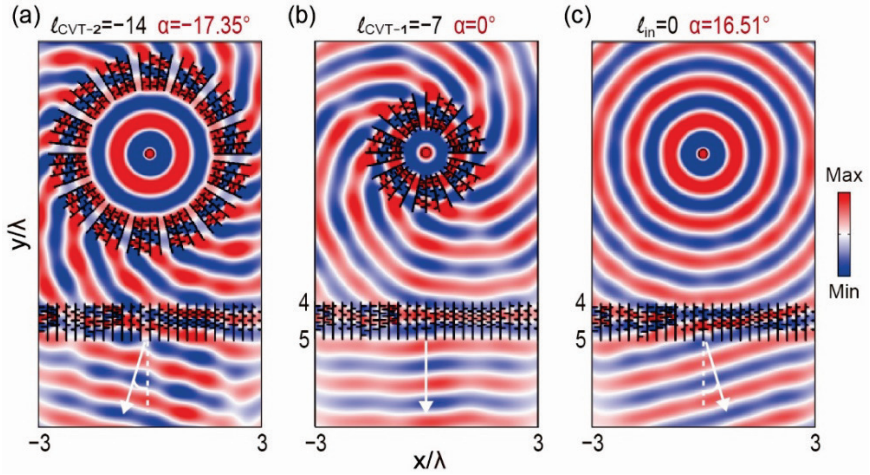

Fig. S4 The experimental simulation field patterns of vortex waves with **(a)** l_{CVT-2}=-14, α=-17.35°; **(b)** l_0=l_{CVT-1}=-7, α=0°; **(c)** l_{in}=0, α=16.51°.

Section 4: The acoustic experimental results for vortex wave with the OAM of 7 and 14

In fact, we do not only measure the control effect of the AM sample on vortex sources with OAM of -14, -7, and 0 as mentioned in the main text, but also obtain the experimental results of incident vortex waves with OAM of 7 and 14 as additional verification, as shown in Fig. S5. Here, we denote the vortex converters generating vortex wave with OAM of 7 and 14 as CVT-3 and CVT-4 respectively, and they are formed by arranging 7 and 14 supercells in an anticlockwise annular arrangement. Specifically, when the vortex source with OAM of 7 generated by CVT-3 goes through the AM sample, the conversion of vortex wave into plane wave with the deflection angle of 32.72° could be observed, as shown in Fig. S5(a). By further increasing the OAM of the incident vortex wave to 14, the vortex wave generated by CVT-4 is smoothly converted into the plane wave with deflection angle of 49.83°, as shown in Fig. S5(b). It is worth mentioning that for vortex waves with OAM of 7 and 14, the deflection angles still satisfy the proposed formula in the main text. Therefore, this further confirms the correctness of our conclusion that AM can efficiently convert vortex waves with arbitrary OAM to plane waves. The foundational principles of this study are relevant to both two-dimensional and three-dimensional vortex wave research systems, with potential applications in particle manipulation and OAM-based detection.

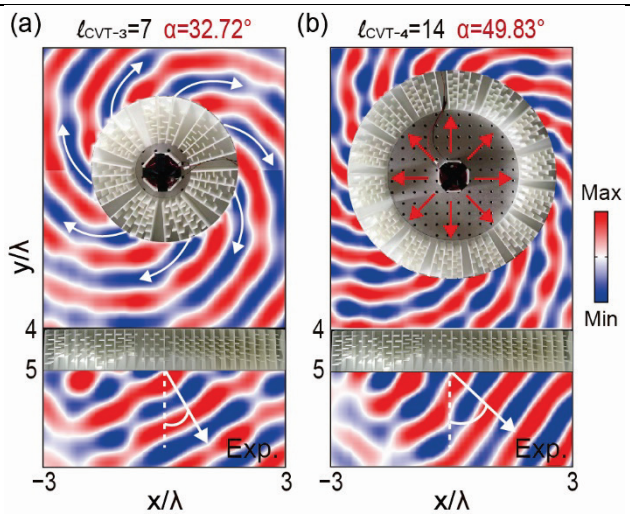

Fig. S5 The experimental demonstration for the efficient conversion of vortex wave with OAM of 7 and 14. The experimental total field patterns of vortex wave with **(a)** l_{CVT-3}=7, α=-32.72°; **(b)** l_{CVT-4}=14, α=49.83°.

References

1. H. Chen and C. T. Chan, Acoustic cloaking in three dimensions using acoustic metamaterials, *Appl. Phys. Lett.* 91, 183518 (2007)
2. S. A. Cummer and D. Schurig, One path to acoustic cloaking, *New J. Phys.* 9, 45 (2007)
3. Y. Li, S. Qi, and M. B. Assouar, Theory of metascreen-based acoustic passive phased array, *New J. Phys.* 18, 043024 (2016)
4. S. Chen, Y. Fan, F. Yang, K. Sun, Q. Fu, J. Zheng, and F. Zhang, Coiling-up space metasurface for high-efficient and wide-angle acoustic wavefront steering, *Front. Mater*. 8, 790987 (2021)
5. Y. Fu, C. Shen, Y. Cao, L. Gao, H. Chen, C. T. Chan, S. A. Cummer, and Y. Xu, Reversal of transmission and reflection based on acoustic metagratings with integer parity design, *Nat. Commun.* 10, 2326 (2019)